

LMI-Based Approach for Regulating Microgrids Using Sliding Mode Control

Mohammed Y. Yakoob¹ | Mina Salim² | Amir A. Ghavifekr³

Faculty of Electrical and Computer Engineering, University of Tabriz, Tabriz, Iran.^{1,2,3}
Corresponding author's email: m.salim@tabrizu.ac.ir

Article Info

Article type:

Research Article

Keywords:

Islanded Microgrid (IMG),
Slide Mode Control (SMC),
Linear Matrix Inequality (LMI),
Voltage Source Inverter (VSI),
Distributed Generation (DG)

ABSTRACT

Regulating voltage and current signals in microgrids (MG) is essential to ensure stability, optimize power quality, support grid integration, enhance operational efficiency, and promote safety within the system. This paper introduces a novel Linear Matrix Inequalities (LMI)-based approach aimed at regulating voltage and current signals within microgrids through the utilization of sliding mode control. The MG under examination in this paper is composed of a voltage source inverter (VSI) for DC to AC voltage conversion, a filter to ensure sinusoidal signal quality, and an array of loads, including those with uncertain characteristics. The objective of this study is to regulate the output voltage and current in a short period of time in the presence of diverse loads. By promptly adjusting voltage and current levels, the microgrid can effectively accommodate fluctuations in demand and maintain optimal performance under changing conditions. The presented controller consists of two parts: a state feedback gain calculated from the LMI and a sliding mode-based controller to maintain system stability. This controller is intended to reject disturbances, track reference signals, and minimize steady-state errors in a limited time. The satisfactory performance of the microgrid will have a significant impact on various parameters, such as frequency, active power, reactive power, and power factor. Simulating the voltage source inverter and presenting numerical results demonstrate the effectiveness of the proposed controller to provide high robustness against uncertainty and nonlinear loads while maintaining system stability.

I. Introduction

In recent years, distributed generation systems have gained the attention of numerous researchers. This is due to the increasing global demand for energy, the high costs associated with traditional energy sources, and the adverse

environmental effects stemming from conventional operations. Consequently, numerous countries have initiated a transition from traditional methods to renewable energy sources such as photovoltaic, wind turbines, and solar thermal systems [1]. Distributed generation and microgrids are closely related concepts in the field of

decentralized energy systems. Distributed generation refers to small-scale power generation facilities that are located close to the point of consumption. Microgrids, on the other hand, are localized energy systems that can operate independently or in connection with the main power grid [2]. Distributed generators form the foundation for enhancing the performance of the power grid and enabling efficient power management within smart networks [3]. In recent years, developers are increasingly focusing on enhancing microgrid functionality to attain superior efficiency and performance [4]. There are numerous benefits to apply a microgrid in a distribution power system (DPS). For instance, it can reduce losses, facilitate the utilization of renewable energy, and enhance system reliability. Furthermore, several factors, such as the remote location of the main grid from urban areas, its high cost, and the complexity of connecting to it, have contributed to the adoption of microgrids in standalone mode[5].

Fig. 1 depicts the basic diagram of the islanded microgrid (IMG) and its architecture. The MG constitutes a single, controllable, independent power system comprising distributed generation (DG), load, energy storage (ES), and control devices, with DG and ES directly connected to the user side in parallel. On the microgrid side, it can be considered a controlled cell, while on the user side, it can fulfill unique demands, such as reduced feeder loss and increased local reliability. With capabilities for autonomous control, protection, and management, a microgrid can operate either in parallel with the main grid or in islanded mode [6].

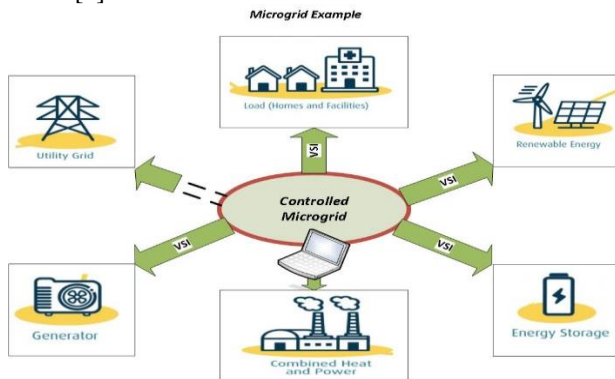


Fig. 1. Microgrid Architecture

Voltage and current signals regulation play a critical role in the reliable and efficient operation of microgrid systems. It is essential for ensuring stability, maintaining power quality, supporting grid integration, optimizing system operation, and promoting safety. Stable voltage and current levels are crucial for the reliable operation of connected loads and equipment, while proper regulation helps prevent issues such as harmonic distortions, which can affect the performance of sensitive electronic devices [7]. Additionally, regulated voltage and current facilitate the smoother integration of microgrids with the main utility grid or other distributed energy resources, ensuring efficient power exchange and grid stability. Precise control of these

signals enables operators to optimize the utilization of distributed energy resources, enhance system efficiency, and reduce operating costs[8]. Thus, a significant challenge lies in obtaining high-quality voltage and current waveforms from microgrids. The Voltage Source Inverter (VSI) plays a critical role in microgrids, and effectively controlling it poses a substantial endeavor.

It is important to use control strategies with MG's in order to control the voltage and current signals' shape and frequency, as well as correct the active and reactive powers [9]. The most commonly used technique is the PID controller, which enables fast response times and minimizes overshoot. In [10], it is noted that PI controllers do not perform well in unbalanced systems. In cases with varying loads, the system's characteristics do not exhibit a consistent transfer function. To overcome this issue, hysteresis controllers have been developed. These controllers are utilized in grid-connected mode, where it ensures that the grid current tracks a reference signal. The key attributes of these controllers include simplicity, robustness, and a favorable transient response. However, a drawback of them is the switching frequency's dependence on load parameters. Another extension is droop controller which has been utilized to stabilize the grid voltage and frequency. The selection of a controller gain depends on the balancing power criteria. Usually, it is used with more than one inverter in parallel. In [11], by using this controller, the MG can achieve active and reactive power balancing. It controls the active and reactive power on the basis of frequency and voltage droop control methods. [12] introduces an adaptive cooperative energy management scheme based on droop control for an autonomous DC microgrid powered by photovoltaic (PV) batteries. Additional emphasis is placed on achieving optimal voltage regulation to enhance robustness against time-delay, as opposed to conventional voltage observers that often result in significant observation errors. Also, Evolutionary algorithms techniques have been applied for the optimal tuning of parameters of these controllers[13]. In [14], an improved state feedback control approach is proposed for the distributed secondary voltage and frequency control within an islanded microgrid. The innovative controllers synchronize the output voltages and frequencies of distributed generators with their reference values. A scheme based on the adaptive input-output feedback linearization control has been proposed in [15]. Implementing the devised control scheme ensures that the output voltage of distributed generation (DG) sources exhibits negligible harmonics. Moreover, it effectively tracks the references for generated voltage, active power, and reactive power.

Sliding mode control (SMC) has emerged as a promising technique for enhancing the performance and stability of microgrids, offering robust and adaptive control capabilities. [16] introduces a novel power control strategy for microgrids based on sliding mode techniques. Compared to the PI controller, the proposed control strategy exhibits a fast response and the capability to closely follow

a reference signal with minimal steady-state error. A novel method based on LMI, has been proposed in [17] for designing decentralized control, specifically targeting large-scale systems. The efficacy of this approach is demonstrated through its application to interconnected clusters of microgrids. To enhance energy extraction from the PV system, [18] introduces a novel controller design strategy aimed at tracking the Maximum Power Point (MPP) utilizing a sliding mode control method for self-optimization. The proposed controller design ensures rapid and precise convergence to the MPP under steady-state conditions and during fluctuations in environmental parameters. A centralized robust sliding mode controller is proposed in [19] aiming to minimize frequency deviation while optimizing power distribution among distributed generations within an isolated microgrid. [20] introduces distributed predictive control implemented at the secondary level of microgrids. The controller proposed takes into account the objectives of frequency and voltage regulation, as well as achieving consensus on the real and reactive power contributions from each power unit within the microgrid. [21] presents a novel approach to decentralized and communication-free control strategies for regulating frequency and voltage in (PV)-Storage islanded Microgrids. In [22], an adaptive sliding mode controller has been designed with a single-phase MG to stabilize the voltage, frequency, and power of the output. Also, in [23], a recursive fast terminal sliding mode controller is presented to regulate a single-phase IMG, where the test is done with a low-voltage grid and is used to stabilize the voltage output by tracking the reference and reducing the error rate between the output and the reference signals. Furthermore, [24] presents an advanced exponential sliding mode controller for microgrids in autonomous and grid-connected modes that outperforms other controllers in terms of fixing a voltage and frequency at the distributed-generated system's common coupling point (CCP). The desired controller for the MG system, should be cheap and easily implementable. It should guarantee the closed loop's stability and have robustness against a wide range of uncertainties and disturbances. In addition, it would be usable to regulate both of the single-phase MG and the three phase MG, to give the pure shape of the voltage and current signals, to provide a high-power factor, get a stable frequency over time, and correct the active and reactive powers. The purpose of this paper is satisfying these conditions by presenting an LMI approach to regulate microgrid voltage and current signals by utilizing sliding mode controller. The proposed controller collects all the properties of the aforementioned scheme and utilizes the compound techniques of SMC and LMI, to provide high robustness against the load variant and uncertainties. The system is asymptotically stable, and the tracking errors converge to zero in finite time. Our study contributes significantly to the existing literature by proposing a novel approach that combines Linear Matrix Inequalities with sliding mode control techniques for regulating microgrids. This integration of LMI methods with sliding mode control

offers a systematic and robust framework for addressing the challenges of microgrid regulation, providing advantages over traditional approaches.

In a summary, this paper is organized as follows: In section 2, the modeling of a single and three-phase autonomous mode MG is presented, the controller design and its stability proof is provided in section 3. In sections 4, and 5, the simulation and tests of a single and three-phase MG are shown, respectively. And finally, section 6 is presented the conclusion and related feature work.

II. Islanded Microgrid and Modelling System

For a microgrid to ensure satisfactory performance and stability, it must be equipped with a proper configuration and structure. The parameters of the proposed MG are mentioned in table (1). For modeling purposes, the system can be divided into two categories: single phase IMG and three phase IMG.

A. Single Phase Islanded Microgrid

Single phase MG is modeled based on the inductor current (i_L) in the L-C filter as shown in Fig. 2.

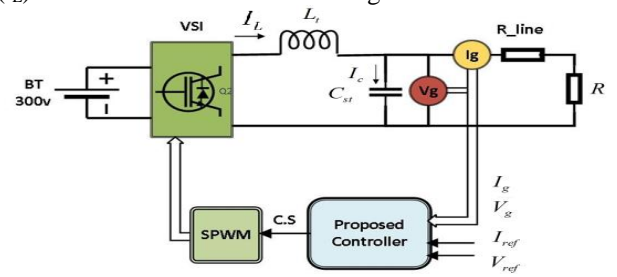


Fig. 2. Single Phase Microgrid Structure

The inductor current is divided into (i_c) and (i_g), and the controller design is based on:

$$L_f \frac{di_L}{dt} = v_{sw} - v_g \quad (1)$$

Where the v_{sw} is implementation of the switching voltage over the sine-wave pulse width modulation (SPWM), and v_g is the grid voltage.

Also, the capacitance current can be written as:

$$i_c = C_{st} \frac{dv_g}{dt} \quad (2)$$

From equations (1) and (2), the state space model can be written as in equation (3).

$$\frac{dx}{dt} = Ax + Bu + d\omega \quad (3)$$

$$y = Cx + Du$$

Where x is the state vector, u is the input vector, and ω is the exogenous input vector of the MG. d is defined as the disturbance vector. This disturbance is considered due to the unknown configuration of the MG and is associated with the grid current. Any change of the MG parameters can happen, which causes the unknown MG configuration and also the unknown grid current and voltage. The state

vector, input vector, and disturbance vector of the MG are shown below:

$$x = \begin{bmatrix} i_L \\ v_g \end{bmatrix}; \quad u = [v_{sw}]; \quad d = [i_g] \quad (4)$$

The state space form is shown in equation (5) as:

$$\frac{d}{dt} \begin{bmatrix} i_L \\ v_g \end{bmatrix} = \begin{bmatrix} 0 & -1 \\ \frac{1}{C_{st}} & 0 \end{bmatrix} \begin{bmatrix} i_L \\ v_g \end{bmatrix} + \begin{bmatrix} \frac{1}{L_t} \\ 0 \end{bmatrix} [v_{sw}] + \begin{bmatrix} 0 \\ -1 \\ \frac{1}{C_{st}} \end{bmatrix} [i_g] \quad (5)$$

And the output of the system is defined in equation (6) as:

$$y = [v_g] = [0 \quad 1] \begin{bmatrix} i_L \\ v_g \end{bmatrix} \quad (6)$$

B. Three Phase Isolated Microgrid

The modeling of three phase MG in Fig.3. can be derived as:

$$v_{t,abc} = L_t \frac{di_{t,abc}}{dt} + R_t i_{t,abc} + v_{abc} \quad (7)$$

$$i_{t,abc} = C_{st} \frac{dv_{abc}}{dt}$$

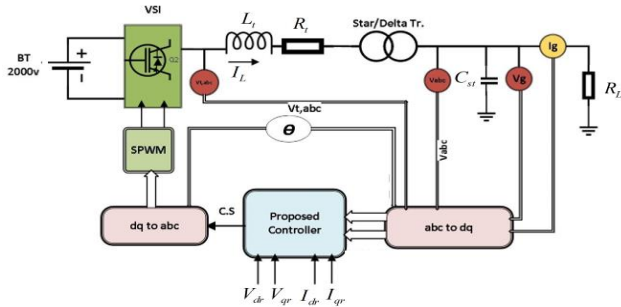


Fig. 3. Three Phase Microgrid Structure

The modeling system in (7) can transfer from abc-frame to $\alpha\beta$ - reference frame as:

$$\frac{d(i_{t,\alpha\beta})}{dt} = -\frac{R_t}{L_t} i_{t,\alpha\beta} - \frac{v_{\alpha\beta}}{L_t} + \frac{v_{t,\alpha\beta}}{L_t} \quad (8)$$

$$\frac{d(v_{\alpha\beta})}{dt} = \frac{i_{t,\alpha\beta}}{C_{st}}$$

And finally, the equation in (8) is converted to a dq-rotating frame and the result in:

$$\frac{d(I_{t,dq})}{dt} + sI_{t,dq} = -\frac{R_t}{L_t} I_{t,dq} + \frac{V_{t,dq}}{L_t} - \frac{V_{dq}}{L_t} \quad (9)$$

$$\frac{d(V_{dq})}{dt} + sV_{dq} = \frac{i_{t,dq}}{C_{st}} \quad (10)$$

where: $s = j\omega_o$.

The state-space model of the open-loop three-phase MG is represented in (9) and (10) is written as the state-space model in (3) and (4). The state space matrices are written as:

$$A = \begin{bmatrix} 0 & W_0 & \frac{1}{C_t} & 0 \\ -W_0 & 0 & 0 & \frac{1}{C_t} \\ -\frac{1}{4} & 0 & -\frac{R_t}{L_t} & W_c \\ 0 & -\frac{1}{L_t} & W_0 & -\frac{R_t}{L_t} \end{bmatrix};$$

$$B = \begin{bmatrix} 0 & 0 & -\frac{1}{C_t} & 0 \\ 0 & 0 & 0 & -\frac{1}{C_t} \\ \frac{1}{4} & 0 & 0 & 0 \\ 0 & \frac{1}{4} & 0 & 0 \end{bmatrix}; \quad C = \begin{bmatrix} 1 & 0 & 0 & 0 \\ 0 & 1 & 0 & 0 \\ 0 & 0 & 1 & 0 \\ 0 & 0 & 0 & 1 \end{bmatrix}; \quad (11)$$

x is the state vector, u is the input vector, and d is the disturbance vector, of the MG that are shown below:

$$x = \begin{bmatrix} V_d \\ V_q \\ I_{td} \\ I_{tq} \end{bmatrix} \quad u = \begin{bmatrix} V_{td} \\ V_{tq} \\ I_{Ld} \\ I_{Lq} \end{bmatrix} \quad d = \begin{bmatrix} V_{gd} \\ V_{gq} \\ I_{gd} \\ I_{gq} \end{bmatrix} \quad (12)$$

III. Controller Design Based on LMI Approach

The proposed controller is guaranteed to be asymptotically stable and the tracking errors will lead to zero. Firstly, depending on the state space model as written in (3) and (10) for single and three-phase MG models, the stability of the sliding mode controller based on LMI is proven by using Lyapunov theory.

The tracking error is defined as:

$$z = x - x_r \quad (13)$$

Where x_r is the desired value.

By assuming the Lyapunov equation as

$$v = z^T P z \quad (14)$$

The controller signal is $u = u_{ARE} + u_r + u_s$.

u_{ARE} : The state feedback gain ($u = kx$), that calculating by solving the Algebraic Ricatii Equation (ARE) by using LMIs.

u_r : The desired control gain. u_s : The switching control signal.

$$u_{ARE} = kx = R^{-1} B^T P x \quad (15)$$

$$u_r = -R^{-1} B^T P x_r - B^{-1} A x_r + B^{-1} \frac{dx_r}{dt} \quad (16)$$

$$u_s = -B^{-1} \eta \text{sign}(z) \quad (17)$$

where η is the amplitude value of the sign function.

In proposed simulation, the $\text{Sign}(\cdot)$ function is replaced by $\text{Sat}(\cdot)$ to reduce the chattering effect and some errors that

are caused by using $Sign(.)$ function. The $Sat(.)$ will be implemented as shown in Fig. (4).

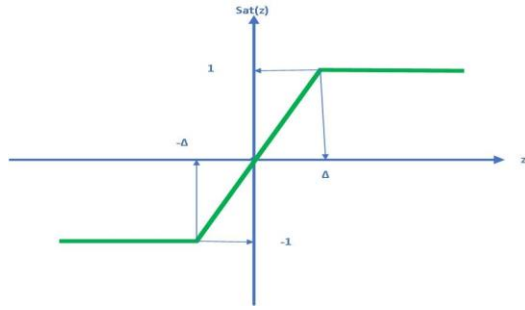


Fig 4. Saturation function implementation

We can obtain a close loop equation by substituting the controller signal in the state space equation:

$$\frac{dx}{dt} = Ax + B(u_{ARE} + u_r + u_s) + d \quad (18)$$

Then, the closed loop system equation will be:

$$\frac{dx}{dt} = Ax + B(R^{-1}B^T Px - R^{-1}B^T Px_r - B^{-1}Ax_r + B^{-1}\frac{dx_r}{dt} - B^{-1}\eta sign(z)) + d$$

The derivative of the Lyapunov equation in (14) is

$$\frac{dv}{dt} = \frac{dz^T}{dt} Pz + z^T P \frac{dz}{dt} \quad (19)$$

And the derivative of the tracking error equation in (13) gets the equation below in (20):

$$\frac{dz}{dt} = \frac{dx}{dt} - \frac{dx_r}{dt} \quad (20)$$

By substantiation (18) into equation (20):

$$\frac{dz}{dt} = Ax + B(u_{ARE} + u_r + u_s) + d - \frac{dx_r}{dt} \quad (21)$$

The next equation has two parts that are obtained from substitutes in the derivative of the Lyapunov equation. The first part will be equal to:

$$-\eta sign(z) + d \quad (22)$$

and that part will be guaranteed to be equal or less than zero by putting the $\eta \geq |d|$ where $|d|$ is the absolute value of the disturbance vector.

The second part will be as follows:

$$(Az + BR^{-1}B^T Pz)^T Pz + z^T P(Az + BR^{-1}B^T Pz) \quad (23)$$

However, the Lyapunov equation guarantees that any system will be asymptotically stable if and only if:

$$A^T P + PA \leq -Q \quad (24)$$

From [25], the algebraic ricatti equation in (23) guarantees the stability of the MG system if and only if

$$(A^T P + PA + Q)/2 + PBR^{-1}B^T P \leq 0 \quad (25)$$

Now, by applying the Shur lemma[26], we will get the inequality below:

$$\begin{bmatrix} (A^T P + PA + Q)/2 & PB \\ B^T P & -R \end{bmatrix} \leq 0 \quad (26)$$

By using LMI in MATLAB, the equation (26) is solved to get the state feedback gain ($k = R^{-1}B^T P$), and the parameters ($P = P^T > 0$), ($R > 0$), and ($Q \geq 0$).

IV. Performance and Simulation Results for the Single-Phase MG

In general, the design of the proposed controller is explained in some steps:

Step 1: We use LMI in MATLAB (YALMIP toolbox) to solve the inequality equation in (26) as a single-phase or three-phase model.

Step 2: In single-phase MG, we chose a sinusoidal as the voltage and current reference signal. But with three-phase MG, the references are 0.6 and 0.8 for voltage and current as dq-frame.

Step 3: The controller component will be implemented using equations (15), (16), and (17).

Step 4: We implement the MG plant and add the disturbances that come from the grid's voltage and current as shown in Figs. (2) and (3).

Table 1. Parameters of the single-phase and three Phase IMG

Parameter	1Phase MG	3Phase MG
DC Battery (v_{dc})	300v	2000v
Inductor Filter (L_f)	2mH	100mH
Shunt Capacitance C_{st}	15 μ F	100 μ F
Resistance of the Line (R_{Line})	0.45 Ω	
Consumer Load (R_L)	40 Ω	40 Ω
Frequency (f)	50Hz	50Hz
MG terminal Voltage (Line to Line)	300v	400v
Transformer Voltage Ratio (Y/ Δ)		12.4/3.4
SPWM Carrier Frequency (f_{sw})	6000 kHz	6000 kHz
Distributed Generation Rated Power		3MV A

Step 5: In this step, the VSI is programmed to rely on Figs. (2) and (3) by tacking the control signal to supply the Sinusoidal Pulse Width Modulation (SPWM), which will activate the VSI.

Step 6: Finally, draw the plant's outputs, which should be similar to the references. Also, the voltage and current output signals should be plotted to show the performance of the controller with the MG.

The single-phase IMG in Fig.2. is designed and the

parameters are taken from the table (1). However, the first implementation is presented with $40\ \Omega$ as the resistive load. Where the reference signals are implemented in a sinusoidal wave with 1 as amplitude and 50Hz . The state feedback gain (k) in (27) is determined by using the LMI technique where Q is chosen to be (2×10^{-6}) . The parameters of the switching function $Sign(\cdot)$ or $Sat(\cdot)$ are chosen as $\eta = [10;300]$. The simulation results are shown in figures (5-A, B, C, and D), which act as the current control signal, the voltage control signal of the presented controller, the current reference and current output, and the voltage reference and voltage output of the plant, respectively. Figures (7-A and B) represent the voltage output and current output of the MG, respectively. From the results, we can show that the presented controller against the resistive load with the MG model has a high performance where the outputs of the plant track the reference signals and the output of the MG is admissible. While the MG's performances against the different loads are shown below:

$$k = \begin{bmatrix} -4.1924 \times 10^4 & 344.1670 \\ -4.0027 \times 10^3 & 4.1702 \times 10^3 \end{bmatrix} \quad (27)$$

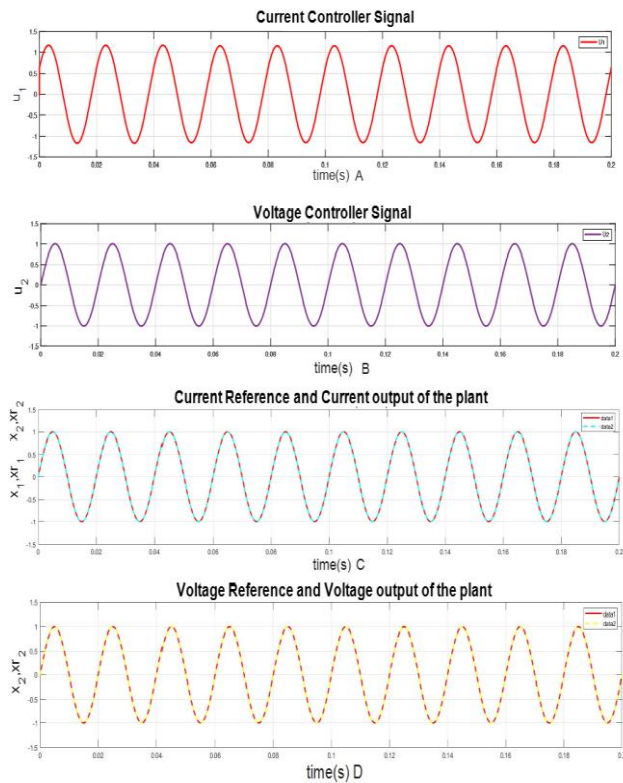


Fig. 5. Controller signals and output of the plant, (A) Current control signal (B)Voltage control signal, (C) Current reference and current output signals, (D)Voltage reference and voltage output signals

A. Performance Against the Unknown Loads

In Fig.6.A, the unknown loads are connected to the single-phase IMG system, and the proposed controller is simulated

in the presence of them. The simulation is completed within 0.2 seconds, with the load changing within 0.1 seconds upon closing the switch. The state feedback gain (k) in (28) is evaluated by using the LMI technique where Q is chosen to be (2×10^{-6}) . The switching function $Sign(\cdot)$ or $Sat(\cdot)$ are chosen as $\eta = [10;300]$. All the results for this test are shown in figures (5-A, B, C, and D) implement the current control signal, the voltage control signal of the proposed controller, the output current, and the output voltage of the plant, respectively. Also, the figures (8-C and D) are the voltage output and current output of the IMG.

$$k = \begin{bmatrix} -4.1924 \times 10^4 & 344.1670 \\ -4.0027 \times 10^3 & 4.1702 \times 10^3 \end{bmatrix} \quad (28)$$

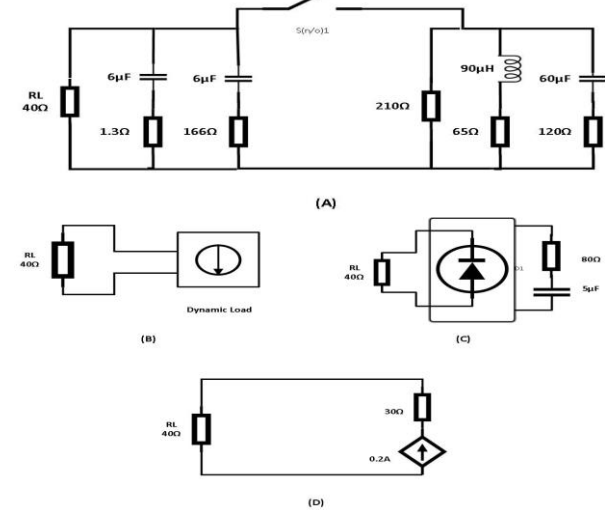


Fig. 6. Types of Different Loads in MG, (A) Unknown Loads, (B) Dynamic Load, (C) Harmonic Load (D)Nonlinear Load

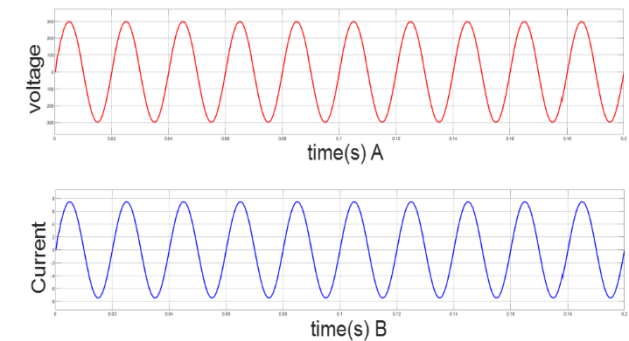


Fig. 7. The output of MG with $R_L=40\ \Omega$, the dynamic load, the non-linear load, and the harmonic load (A)Voltage Output and (B) Current Output.

B. Performance Against the Dynamic Load

In this part, the single-phase IMG is simulated against a dynamic load as shown in Fig.6.B with parameters being taken as $(V_{rms} = 300\text{v}, F = 50\text{Hz}, P = 50\text{w}, \text{ and } Q = 2\text{var})$. The state feedback gain (k) in (29) is determined by using the LMI technique. Q is chosen to be (2×10^{-6}) . The parameters of the switching functions $Sign(\cdot)$ or $Sat(\cdot)$ are

chosen as $\eta = [10;300]$. The results are shown in figures (5-A, B, C, and D) for the current control signal, the voltage control signal of the proposed controller, the output current, and the output voltage of the plant, respectively. The dynamic load is added to the MG, and the test happens in 0.2 seconds. We can demonstrate that the proposed controller performs well against dynamic loads, where the plant's output current and voltage track the reference signals, and the MG provides admissible waveforms.

$$k = \begin{bmatrix} -4.1924 \times 10^4 & 344.1670 \\ -4.0027 \times 10^3 & 4.1702 \times 10^3 \end{bmatrix} \quad (29)$$

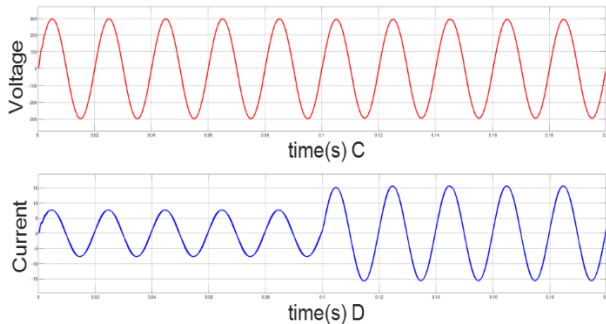


Fig. 8. The output of MG against the unknown loads (C) Voltage Output and (D) Current Output.

C. Performance Against the Non-Linear Load

The nonlinear load in Fig. 5.C is simulated with the single-phase IMG. The time of the simulation is 0.2 seconds, and the nonlinear load is connected to the MG from the beginning. Where the state feedback gain (k) in (30) is calculated by using the LMI technique. Q is chosen to be (2×10^{-6}) . The parameters of the switching functions $Sign(\cdot)$ or $Sat(\cdot)$ are chosen as $\eta = [10;300]$. As shown in the results, the proposed controller works well with the MG model, where the current and voltage outputs track the reference signals. As shown in the results, the proposed controller works well with the MG model, where the current and voltage outputs track the reference signals. In addition, the output voltage and current of the MG have admissible waveforms.

$$k = \begin{bmatrix} -4.1924 \times 10^4 & 344.1670 \\ -4.0027 \times 10^3 & 4.1702 \times 10^3 \end{bmatrix} \quad (30)$$

D. Performance Against the Harmonic Load

The single-phase MG is simulated against the harmonic load as shown in figure(6-D), where the current source with 0.2A and $F = 150\text{Hz}$ is added to $R = 30\Omega$. The state feedback gain (k) in (31) is determined by using the LMI technique where Q is chosen to be (10^{-5}) . The parameters of the switching functions $Sign(\cdot)$ or $Sat(\cdot)$ are chosen as $\eta = [10;300]$. All the tests were completed in 0.2 seconds, and the harmonic load was connected for the first time. It was shown that the presented controller has high performance with the MG, where the outputs of the model track the reference signals and the outputs of the MG have admissible waveforms.

$$k = \begin{bmatrix} -1.4795 \times 10^5 & 1.877 \times 10^3 \\ -1.3039 \times 10^4 & 3.1641 \times 10^4 \end{bmatrix} \quad (31)$$

E. Performance Against the Compound Loads

In this section, the test with a single-phase MG is simulated against the compound loads with the same specifications as in the above tests. In figures (6-C, A, and D) the proposed controller, for the resistive load $R_L = 40$ is connected from the first time. At time 0.01 seconds, the nonlinear load is added; at time 0.03 seconds, the unknown loads are connected; the switch is closed at time 0.07 seconds, and the harmonic load is added at time 0.1 seconds. Where the state feedback gain (k) in (32) is evaluated by using the LMI technique where Q is chosen to be (10^{-5}) . The parameters of the switching function $Sign(\cdot)$ or $Sat(\cdot)$ are chosen as $\eta = [16;305]$. Reference signal and voltage output of the MG model, shown in Fig. 9, where the output voltage is shown in (K) and (L) is presented as the output current of the MG. From the results, the outputs of the MG model with the proposed controller track the reference signals, and the outputs of the MG give admissible waveforms.

$$k = \begin{bmatrix} -1.4795 \times 10^5 & 1.877 \times 10^3 \\ -1.3039 \times 10^4 & 3.1641 \times 10^4 \end{bmatrix} \quad (32)$$

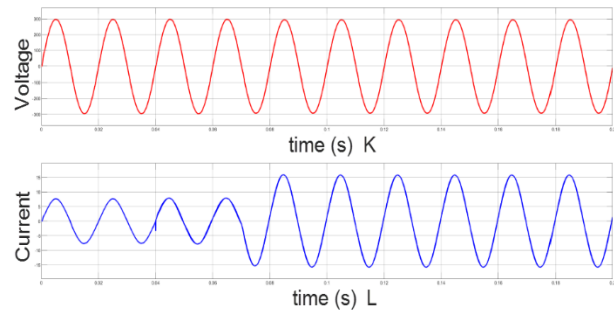


Fig. 9. The output of MG against the compound load (K) Output voltage and (L) Output current.

V. Performance and Simulation Results for the Three Phase MG

Three-phase IMG is simulated with the proposed controller, as shown in Fig. 3. The references for the voltage and current are chosen to be 0.6DC for a V_d and I_d and 0.8DC for a V_q and I_q in the dq -frame to be similar to the three phase signals in abc -frame. The angle Θ is calculated in the second step by integrating W_o , where W_o equals to $(2\pi f)$. Where the state feedback gain (k) in (33) is calculated by using the LMI technique. The parameters of the switching function $Sign(\cdot)$ or $Sat(\cdot)$ are chosen as $\eta = [350;200;6;0.5]$. However, all of the tests performed in this section are compared to papers such as [27-29], and [30] to demonstrate that the performance of the proposed controller is better. So, we start the simulation with $R_L = 40$ connected as the first terminal to the lines of the MG and the other terminal to the ground. The test is applied for 0.2 seconds, and the resistive load is connected for the first time.

Figures (12-A, B, C, and D) show the controller's input as a reference, the output voltage and current of the MG plant in a dq -frame, the voltage control signal, and the current control signal of the proposed controller, in that order. Also, what shown in the figures (13-E, F, G, and H) are the outputs of the three-phase MG: voltage, current, active power, and reactive power, respectively. There are some tests that are performed with the three-phase MG and the proposed controller, as shown below.

$$k = \begin{bmatrix} -1.1 \times 10^4 & 1.15 \times 10^4 & -1.96 \times 10^7 & 8.2 \times 10^4 \\ -3.66 \times 10^4 & -2.5 \times 10^4 & 1.04 \times 10^5 & -1.9 \times 10^7 \\ 1.8 \times 10^7 & 1.6 \times 10^4 & -3.9 \times 10^4 & 9.6 \times 10^4 \\ 1.6 \times 10^4 & 1.8 \times 10^7 & -1.7 \times 10^4 & 3.14 \times 10^4 \end{bmatrix} \quad (33)$$

A. Performance Against the Unknown Loads

The second test is done by connecting the three phase unknown loads as shown in figure (6-A), where the first part is from the $R_L = 40\Omega$ side. The first terminal is connected to the first phase line of the MG, and the second terminal is connected to the ground. Then it is repeated with every phase. Also, the second part is added in the same way after a three-phase switch, with a three-phase MG and the proposed controller, where the simulation happens for 0.2 seconds and the switch is closed at 0.1 second. The state feedback gain (k) in (34) is determined by using the LMI technique. The parameters of the switching function $Sign(\cdot)$ or $Sat(\cdot)$ are chosen as $\eta = [300; 200; 11; 1]$. The results are shown in figures (12-A and B) which represent the plant output voltage and current. In addition, figures (12-C and D) represent the controller voltage and current signals. Moreover, the figures (13-E, F, G, and H) are the voltage, current, active power, and reactive power output of the three-phase MG, respectively.

$$k = \begin{bmatrix} -1.1 \times 10^4 & 1.15 \times 10^4 & -1.96 \times 10^7 & 8.2 \times 10^4 \\ -3.66 \times 10^4 & -2.5 \times 10^4 & 1.04 \times 10^5 & -1.9 \times 10^7 \\ 1.8 \times 10^7 & 1.6 \times 10^4 & -3.9 \times 10^4 & 9.6 \times 10^4 \\ 1.6 \times 10^4 & 1.8 \times 10^7 & -1.7 \times 10^4 & 3.14 \times 10^4 \end{bmatrix} \quad (34)$$

B. Performance Against the Dynamic Load

This section is testing a three-phase IMG against a three-phase dynamic load, where the specifications of the dynamic load as shown in figure (5-B) are $v_{rms} = 400\text{volts}$, $F = 50H_z$, $P = 1000\text{watts}$, and $Q = 20\text{var}$, with the proposed controller. The simulation is presented in real time for 0.2 seconds, and the dynamic load is connected from the beginning. Where the Q is chosen to be 0.65×10^{-7} . The state feedback gain (k) in (35) is evaluated by using the LMI technique.

$$k = \begin{bmatrix} 215.89 & -74.56 & -4.7 \times 10^3 & 1.149 \times 10^3 \\ -186.48 & 265.57 & 1.17 \times 10^3 & -4.68 \times 10^3 \\ 1.28 \times 10^4 & 2.27 \times 10^3 & -2.6 \times 10^3 & 467.387 \\ 2.12 \times 10^3 & 1.8 \times 10^4 & -77.436 & -3.04 \times 10^3 \end{bmatrix} \quad (35)$$

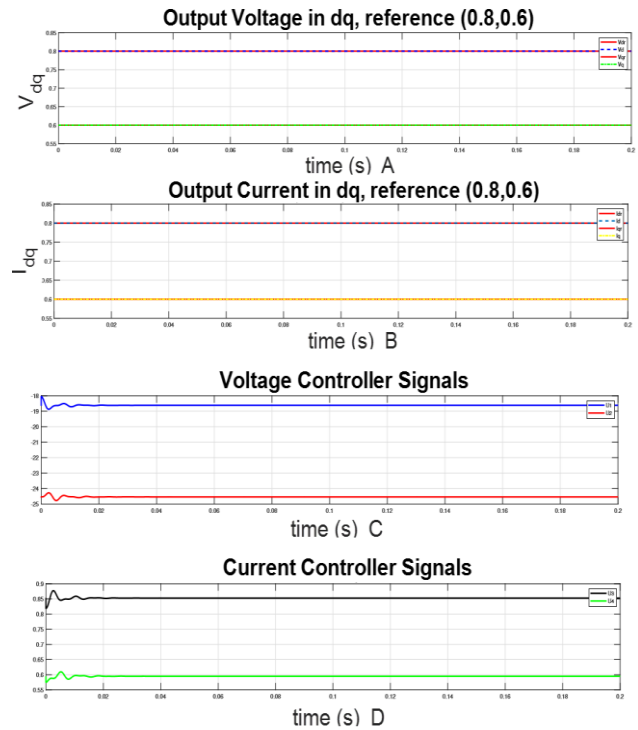


Fig. 10. The input and output of the controller with a MG plant against the resistive load (A-B) Voltage and Current in dq -frame (C-D) Control signals in dq -frame.

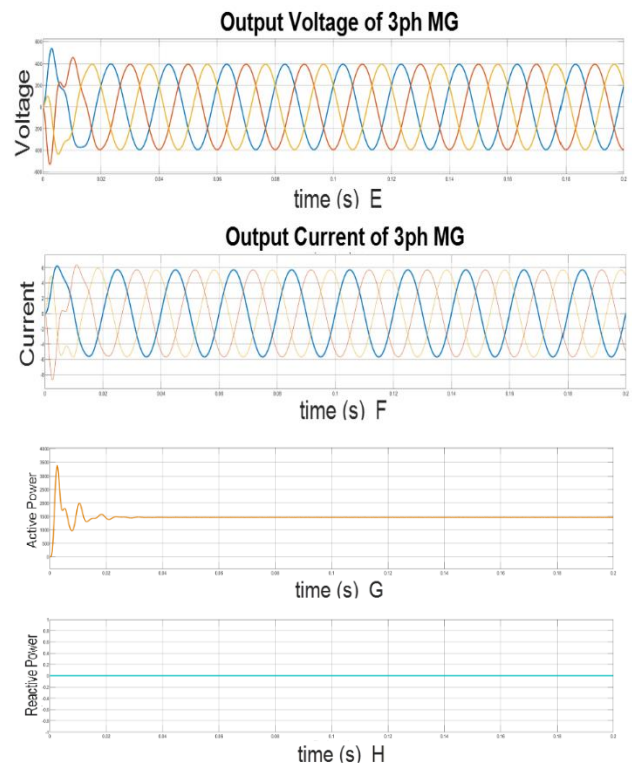


Fig. 11. The output of a three phase MG against the resistive load (E) Voltage Output of the MG (F) Current Output of the MG (G) Active Power Output of the MG, (H) Reactive Power Output of the MG.

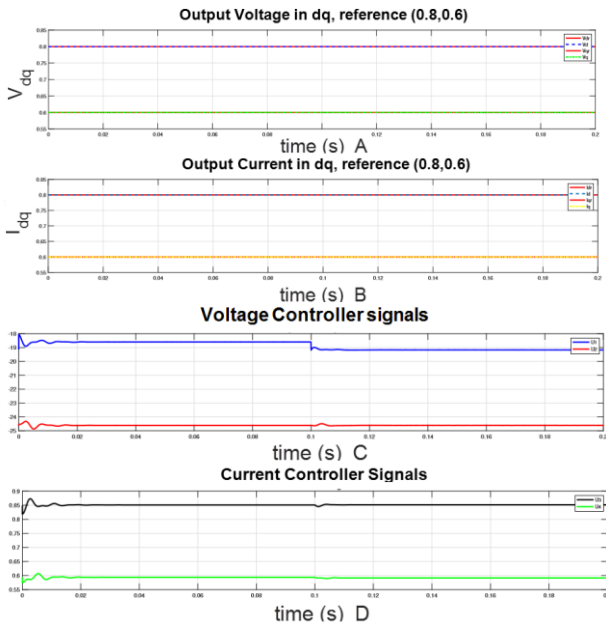


Fig. 12. The input and output of the controller with a MG plant against the unknown loads (A-B) Voltage and Current in dq-frame (C-D) Control signals in dq-frame.

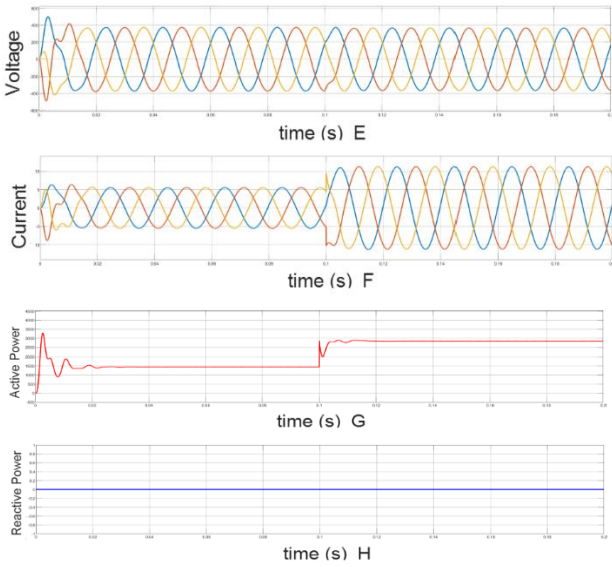


Fig. 13. The output of a three phase MG against the unknown loads (E)Voltage Output of the MG (F) Current Output of the MG (G) Active Power Output of the MG (H) Reactive Power Output of the MG

The parameters of the switching function $Sign(.)$ or $Sat(.)$ are chosen as $\eta = [600;500;5;12]$. However, the results of the test are shown in figures (14-A and B), The voltage and current outputs of the three-phase MG plant in dq - frame and (C, D) are the voltage and current signals of the controller. Moreover, the figures (15-E, F, G, and H) are the output voltage, current, active power, and reactive power of the three-phase MG, respectively. From the above results, we can conclude that the proposed controller is performing well because it has outputs from the MG model that track the reference signals.

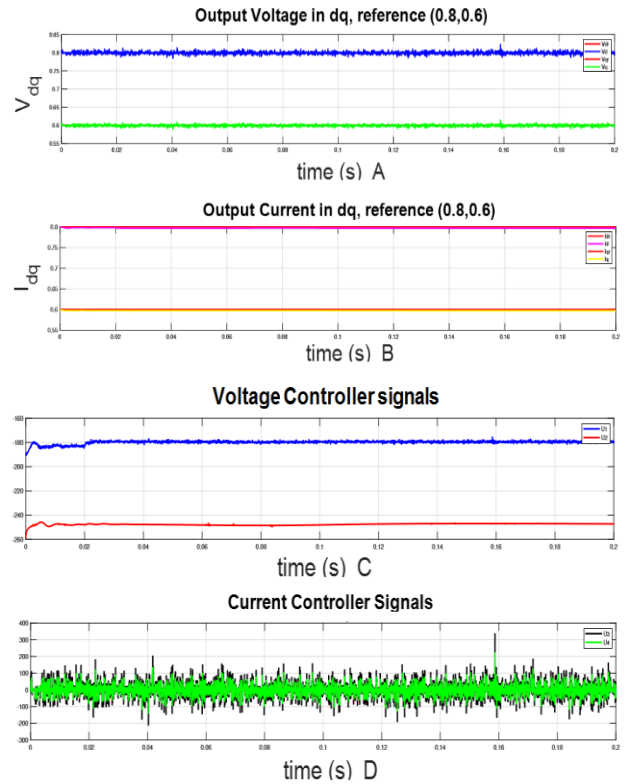


Fig. 14. The input and output of the controller with a MG plant against the dynamic load (A-B) Voltage and Current in dq-frame (C-D) Control signals in dq-frame.

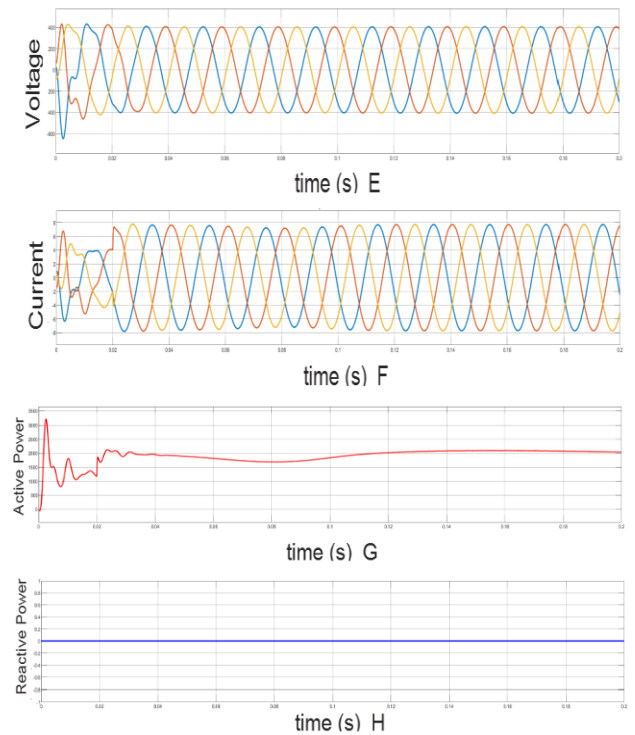


Fig. 15. The output of a three phase MG against the dynamic load (E)Voltage Output of the MG (F) Current Output of the MG (G) Active Power Output of the MG, (H) Reactive Power Output of the MG

C. Performance Against the Non-linear Load

For this test, the three-phase nonlinear load is connected to a three-phase IMG. The simulation was done with $R_L = 40\Omega$ during a time of 0.2 seconds, and the nonlinear load was added at 0.1 second. Where the Q is chosen to be 10^{-5} . The state feedback gain (k) in (36) is calculated by using the LMI technique. The parameters of the switching function $Sign(\cdot)$ or $Sat(\cdot)$ are chosen as $\eta = [300;350;5;10]$. The results are shown in figures (16-A, B, C, and D), the input as reference in the dq - frame, the output voltage, current in the dq - frame of the three phase MG plant, the voltage control signal, and the current control signal output of the proposed controller, respectively. In addition, the figures (17-E and F) are the output voltage and current of the three-phase MG, and (G and H) are the active and reactive power of the MG.

$$k = \begin{bmatrix} -580.2 & -283.2 & -6.1 \times 10^4 & 2.7 \times 10^3 \\ -344.2 & -697.0 & 2.7 \times 10^3 & -1.1 \times 10^4 \\ 6.5 \times 10^4 & -3.7 \times 10^3 & 412.69 & 776.89 \\ -3.6 \times 10^3 & 6.6 \times 10^4 & 933.75 & 703.23 \end{bmatrix} \quad (36)$$

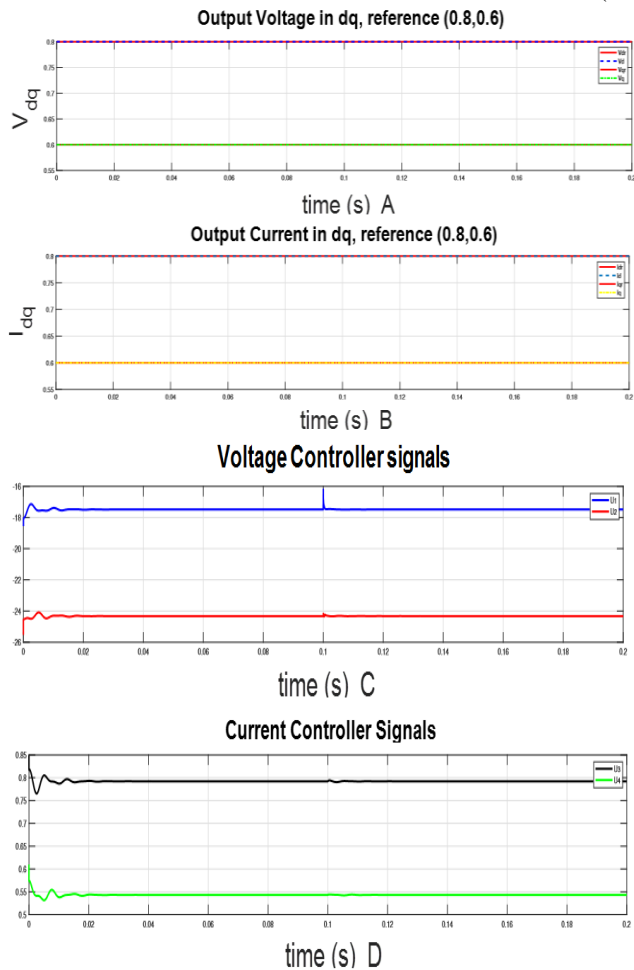


Fig. 16. The input and output of the controller with a MG plant against the nonlinear load (A-B) Voltage and Current in dq-frame, (C-D) Control signals in dq-frame.

D. Performance Against the Compound Loads

The final test is a three-phase IMG, and the proposed controller is against the compound loads. This means all the loads are connected to the MG, where the first $R_L = 40\Omega$ and the dynamic loads are connected at the beginning. The unknown loads are added at 0.03 seconds and the switch is closed at 0.06 seconds. In the third case, the harmonic load is added at 0.1 second, and in the end, the nonlinear load is added at 0.15 second. Where the Q is chosen to be 0.65×10^{-5} . The state feedback gain (k) in (37) is calculated by using the LMI technique. The parameters of the switching function $Sign(\cdot)$ or $Sat(\cdot)$ are chosen as $\eta = [600;500;5;20]$.

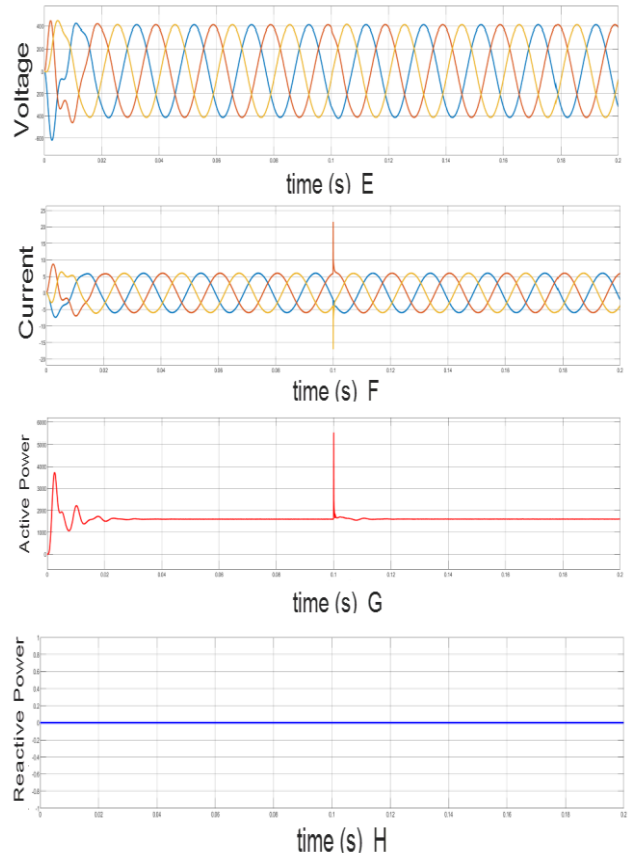


Fig. 17. The output of a three phase MG against the nonlinear load (E) Voltage Output of the MG (F) Current Output of the MG (G) Active Power Output of the MG (H) Reactive Power Output of the MG.

However, the results for 0.2 seconds are shown in figures (18-A, B, C, and D), which are the reference signals in a dq - frame, output voltage, current of the MG plant, voltage, and current control signal of the proposed controller, respectively.

$$k = \begin{bmatrix} 215.89 & -74.56 & -4.7 \times 10^3 & 1.149 \times 10^3 \\ -186.48 & 265.57 & 1.17 \times 10^3 & -4.68 \times 10^3 \\ 1.28 \times 10^4 & 2.27 \times 10^3 & -2.6 \times 10^3 & 467.387 \\ 2.12 \times 10^3 & 1.8 \times 10^4 & -77.436 & -3.04 \times 10^3 \end{bmatrix} \quad (37)$$

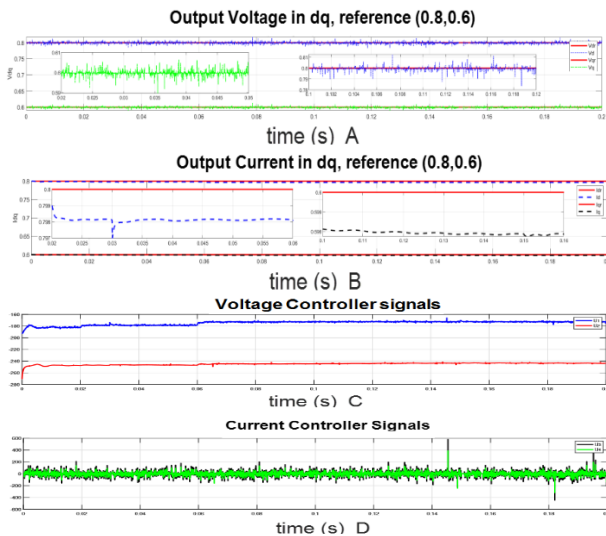


Fig. 18. The input and output of the controller with a MG plant against the compound loads (A-B) Voltage and Current in dq-frame (C-D) Control signal in dq-frame.

As demonstrated in the results, the performance of the proposed controller is deemed acceptable, particularly considering the challenge of managing various loads within the same test scenario. Utilizing the voltage control signal for microgrid regulation proves advantageous due to the dynamic load's impact on the entire system. Consequently, the output waveforms of the microgrid exhibit satisfactory characteristics.

VI. Conclusion

This paper introduces a sliding mode controller utilizing the LMI approach, designed to regulate and optimize both the voltage and current signals in single-phase and three-phase microgrids. The application of the presented controller results in the MG model's output precisely tracking the reference signals, demonstrating the effectiveness and precision of the control strategy in maintaining desired performance levels. Additionally, the output voltage and current signals of the microgrid display acceptable waveforms, while the correction time is notably shorter compared to similar studies. Simulated results demonstrate that the proposed controller can enhance various aspects of the MG's outputs, including active power, reactive power, and power factor. Moreover, the proposed controller is not a complex composite structure when compared to similar counterparts. Future developments of the proposed controller will focus on the LC filter, which will be modified adaptively along with the loads to ensure compatibility with the controller's operation and deliver admissible output waveforms for the MG. Furthermore, because the structure of the proposed controller is not complex and its outputs are voltage and current signals, it can simultaneously regulate two Voltage Source Inverters using a single regulator, which makes the proposed controller more cost-effective. Future work should aim to

develop a controller capable of simultaneously regulating multiple VSIs in a single MG. This advancement would facilitate more efficient utilization of renewable energy sources and enhance the overall performance of the microgrid system.

REFERENCES

- [1] Z. Yang, F. Yang, H. Min, H. Tian, W. Hu, and J. Liu, "Review on optimal planning of new power systems with distributed generations and electric vehicles," *Energy Reports*, vol. 9, pp. 501-509, 2023.
- [2] S. Ahmad, M. Shafiullah, C. B. Ahmed, and M. Alowafeer, "A review of microgrid energy management and control strategies," *IEEE Access*, vol. 11, pp. 21729-21757, 2023.
- [3] S. Vuddanti and S. R. Salkuti, "Review of energy management system approaches in microgrids," *Energies*, vol. 14, no. 17, p. 5459, 2021.
- [4] S. Mizani and A. Yazdani, "Optimal design and operation of a grid-connected microgrid," in *2009 IEEE Electrical Power & Energy Conference (EPEC)*, 2009: IEEE, pp. 1-6.
- [5] R. Bayindir, E. Hossain, E. Kabalci, and R. Perez, "A comprehensive study on microgrid technology," *International Journal of Renewable Energy Research*, vol. 4, no. 4, pp. 1094-1107, 2014.
- [6] F. Li, R. Li, and F. Zhou, *Microgrid technology and engineering application*. Elsevier, 2015.
- [7] M. J. Ghadi, A. Rajabi, S. Ghavidel, A. Azizvahed, L. Li, and J. Zhang, "From active distribution systems to decentralized microgrids: A review on regulations and planning approaches based on operational factors," *Applied Energy*, vol. 253, p. 113543, 2019.
- [8] A. Iovine, M. J. Carrizosa, E. De Santis, M. D. Di Benedetto, P. Pepe, and A. Sangiovanni-Vincentelli, "Voltage regulation and current sharing in DC microgrids with different information scenarios," *IEEE Transactions on Control Systems Technology*, vol. 30, no. 5, pp. 1905-1919, 2021.
- [9] M. H. Andishgar, E. Gholipour, and R.-a. Hooshmand, "An overview of control approaches of inverter-based microgrids in islanding mode of operation," *Renewable and Sustainable Energy Reviews*, vol. 80, pp. 1043-1060, 2017.
- [10] A. M. Bouzid, J. M. Guerrero, A. Cheriti, M. Bouhamida, P. Sicard, and M. Benghanem, "A survey on control of electric power distributed generation systems for microgrid applications," *Renewable and Sustainable Energy Reviews*, vol. 44, pp. 751-766, 2015.
- [11] Y. Sun *et al.*, "An fP/Q droop control in cascaded-type microgrid," *IEEE Transactions on Power Systems*, vol. 33, no. 1, pp. 1136-1138, 2017.
- [12] S. Sahoo, S. Mishra, S. Jha, and B. Singh, "A cooperative adaptive droop based energy management and optimal voltage regulation scheme for DC microgrids," *IEEE Transactions on Industrial Electronics*, vol. 67, no. 4, pp. 2894-2904, 2019.
- [13] M. Ahmadi Kamarposhti, "Optimal control of islanded micro grid using particle swarm optimization algorithm," *International Journal of Industrial Electronics Control and Optimization*, vol. 1, no. 1, pp. 53-60, 2018.

- [14] M. Alizadeh, H. Askarian Abyaneh, A. Bakhshai, and N. Khodabakhshi Javinani, "An Enhanced Distributed State Feedback for Secondary Control in an Islanded Microgrid," *International Journal of Industrial Electronics Control and Optimization*, vol. 5, no. 2, pp. 123-132, 2022.
- [15] N. R. Abjadi, "Adaptive input-output feedback linearization control for islanded inverter-based microgrids," *International Journal of Industrial Electronics Control and Optimization*, vol. 6, no. 3, pp. 183-192, 2023.
- [16] R. Sedaghati and M. R. Shakarami, "A new sliding mode-based power sharing control method for multiple energy sources in the microgrid under different conditions," *International Journal of Industrial Electronics Control and Optimization*, vol. 2, no. 1, pp. 25-38, 2019.
- [17] M. Khanbaghi and A. Zečević, "An LMI-based control strategy for large-scale systems with applications to interconnected microgrid clusters," *IEEE Access*, vol. 10, pp. 111554-111563, 2022.
- [18] Y. M. Alsmadi *et al.*, "Sliding mode control of photovoltaic based power generation systems for microgrid applications," *International Journal of Control*, vol. 94, no. 6, pp. 1704-1715, 2021.
- [19] S. Prasad, "Robust sliding mode controller for frequency regulation in a microgrid," *Transactions of the Institute of Measurement and Control*, vol. 45, no. 10, pp. 1947-1964, 2023.
- [20] J. S. Gomez, D. Saez, J. W. Simpson-Porco, and R. Cárdenas, "Distributed predictive control for frequency and voltage regulation in microgrids," *IEEE Transactions on Smart Grid*, vol. 11, no. 2, pp. 1319-1329, 2019.
- [21] A. Rosini, D. Mestriner, A. Labella, A. Bonfiglio, and R. Procopio, "A decentralized approach for frequency and voltage regulation in islanded PV-Storage microgrids," *Electric Power Systems Research*, vol. 193, p. 106974, 2021.
- [22] U. K. Kalla, B. Singh, S. S. Murthy, C. Jain, and K. Kant, "Adaptive sliding mode control of standalone single-phase microgrid using hydro, wind, and solar PV array-based generation," *IEEE transactions on smart grid*, vol. 9, no. 6, pp. 6806-6814, 2017.
- [23] S. K. Gudey and R. Gupta, "Recursive fast terminal sliding mode control in voltage source inverter for a low - voltage microgrid system," *IET Generation, Transmission & Distribution*, vol. 10, no. 7, pp. 1536-1543, 2016.
- [24] A. Elnady and M. AlShabi, "Advanced exponential sliding mode control for microgrid at autonomous and grid-connected modes," *Bulletin of Electrical Engineering and Informatics*, vol. 10, no. 1, pp. 474-486, 2021.
- [25] B. Carvalho and L. Rodrigues, "Multivariable PID synthesis via a static output feedback LMI," in *2019 IEEE 58th Conference on Decision and Control (CDC)*, 2019: IEEE, pp. 8398-8403.
- [26] C. Olalla, R. Leyva, A. El Aroudi, and I. Queinnec, "Robust LQR control for PWM converters: An LMI approach," *IEEE Transactions on industrial electronics*, vol. 56, no. 7, pp. 2548-2558, 2009.
- [27] M. Armin *et al.*, "Robust extended H_∞ control strategy using linear matrix inequality approach for islanded microgrid," *IEEE access*, vol. 8, pp. 135883-135896, 2020.
- [28] F. R. Badal, P. Das, S. K. Sarker, and S. K. Das, "A survey on control issues in renewable energy integration and microgrid," *Protection and Control of Modern Power Systems*, vol. 4, no. 1, pp. 1-27, 2019.
- [29] M. Y.-Y. U. Haque, M. R. Islam, J. Hasan, and M. R. I. Sheikh, "Negative imaginary theory-based proportional resonant controller for voltage control of three-phase islanded microgrid," *Journal of Control, Automation and Electrical Systems*, vol. 32, pp. 214-226, 2021.
- [30] M. Y.-Y. U. Haque, M. R. Islam, T. Ahmed, and M. R. I. Sheikh, "Improved voltage tracking of autonomous microgrid technology using a combined resonant controller with lead-lag compensator adopting negative imaginary theorem," *Protection and Control of Modern Power Systems*, vol. 7, no. 1, p. 10, 2022.



Mohammed Yousif Yakoob was born in Iraq, in 1983, he received his Bcs from Basra University and Master degree from University of Tabriz, and he is working in Iraqi ministry of electrical, Nasiriyah Thermal Power Station.



Mina Salim was born in Mahabad, Iran in 1983. She received her B.sc in Electrical Engineering from Sahand University of Technology in 2005, Sahand, Iran, and her M.Sc. degree in Electrical Engineering from University of Tabriz, Iran in 2009. She received her Ph. D degree in Electrical Engineering from Sahand University of Technology in 2016. She is currently an Assistant professor in Department of Control Engineering, Faculty of Electrical and Computer Engineering at University of Tabriz, Iran. Her currently interest area are Data Driven Fault Detection and Control Methods and their Application for industrial processes, Robust Control, and Intelligent Algorithms.



Amir.A. Ghavifekr is currently an assistant professor of control engineering at university of Tabriz-Iran. He was studying at University of Tabriz in Electrical –Control Engineering and received his B.Sc. and M.Sc. degrees in Control Engineering in 2009 and 2012. He received his Ph.D. degree in control engineering in the field of Teleoperation systems from university of Tabriz with cooperation of university of Verona in Italy in 2018. His thesis was about “Multi-rate control of Teleoperation systems with Networked Structures”. His research interests are focused on: Teleoperation and Telesurgery, Robotic manipulators, Network Control Systems (NCS), Multi-rate Control, Digital Control, Nonlinear Control, Virtual reality, and also, he has worked on intelligent systems. He has actively engaged with the professional community. Amir is an active Senior member of the IEEE and the member of development committee of IEEE Iran section. Recently he has been selected as the chair of the IEEE young professional committee of Iran section. He has also served several reputable IEEE indexed conferences such as PEDSTC, ICCIA, ICEE and SGC as the executive chair and international relation chair.